Higher-order resonant behavior in asymmetric nonlinear stochastic systems

M. E. Inchiosa* and A. R. Bulsara†
Naval Command, Control and Ocean Surveillance Center, RDT&E Division, Code D364, San Diego, California 92152-5000

L. Gammaitoni‡
Dipartimento di Fisica, Universita di Perugia, I-06100 Perugia, Italy
and Istituto Nazionale de Fisica Nucleare, Virgo Project, I-06100 Perugia, Italy
(Received 18 November 1996)

We study periodically modulated bistable dynamic elements subject to Gaussian noise and a symmetry-breaking dc signal. The skewing of the bistable potential function by the dc signal leads to the appearance of even multiples of the drive frequency in the output power spectral density. The spectral amplitudes of *all* the harmonics are found to exhibit maxima as functions of the noise statistics and the dc signal; the maxima can be shown to depend on matchings of characteristic deterministic and stochastic time scales. A phenomenological description based on a generic bistable system is followed by actual perturbation calculations of the first two spectral amplitudes for a real system, a Josephson junction shorted by a superconducting loop (the mainstay of the rf superconducting quantum interference device). This behavior underlies a recently proposed ''frequency-shifting'' technique for circumventing detector noise limitations which would otherwise constrain the detection of very low-amplitude signals. [S1063-651X(97)05604-3]

PACS number(s): 05.40.+j, 02.50.Fz

I. INTRODUCTION

Periodically modulated stochastic systems have received considerable attention recently [1]; these systems which can generally be described by the ''particle-in-potential'' paradigm, $\dot{x}=-[\partial U(x)/\partial x]+S(t)+N(t)$, exhibit a richness of noise-mediated resonance behavior in the spectral measures [e.g., the output signal-to-noise ratio, (SNR)] of the response. In these systems, $S(t)$ and $N(t)$ denote a deterministic signal (often taken to be time periodic) and noise (usually taken to be Gaussian). The potential function $U(x)$ is even (often bistable), resulting in an output power spectral density (PSD) consisting of *odd* multiples of the signal frequency ω superimposed on a Lorentzian noise background. However, real-world manifestations of these systems are often asymmetric, with the dynamics containing even and odd functions of the state variable. The simplest route to asymmetry in the above dynamics is to incorporate a small dc term x_0 into the signal $S(t)$ or, equivalently, a term $-xx_0$ into $U(x)$. The output PSD of asymmetric systems contains contributions from *all* the harmonics of the periodic signal frequency; hence, the appearance and change in the magnitudes, as a function of x_0, of peaks at even multiples of ω (this would, of course, be accompanied by a concommitant change in the spectral amplitudes at odd multiples) could be taken as quantifying measures of the asymmetry-producing signal. Asymmetric dynamic systems of the above form have been studied [2] with Gaussian white noise. The spectral amplitudes of the harmonics of the periodic signal, in the output PSD, pass through maxima as a function of noise intensity. It has been suggested that this behavior might be a manifestation of the well-known *stochastic resonance* (SR) effect at higher orders [3].

In this work we present a systematic treatment of the resonant behavior of the spectral amplitudes at $k\omega$ ($k=1,2,3\ldots$). The resonant behavior depends on a new control parameter, the degree of asymmetry, and can be interpreted at all orders k, via a matching of deterministic and stochastic time scales reminiscent of recent interpretations of SR in integrate-fire model neurons [4] and bistable dynamic systems [5] as a *bona fide* resonance. We start with a purely deterministic phenomenological theory that shows the occurrence of multiple maxima in the spectral amplitudes in a generic asymmetric system; we then introduce characteristic stochastic time scales (these critically depend on the asymmetry, as well as the spectral characteristics of the noise) and argue that a precise and elegant matching of these time scales must occur for *all* k for there to be resonance behavior in the spectral amplitudes of the harmonics when the noise is turned on. The phenomenological development is followed by a theoretical computation of the first two spectral amplitudes ($k=1,2$) on a rf superconducting quantum interference device (SQUID) loop; results in line with recent experimental observations are obtained, and the resonance behavior as a function of the noise variance (for fixed asymmetry) is also discussed. In a recent publication [6] we have shown numerical simulations of the higher harmonic behavior in the rf SQUID loop to $O(k=4)$ and speculated that these results could be applied to carrying out detection of very weak dc signals in nonlinear sensors that are constrained by noise in well-defined bandwidths; we discuss these points in greater detail in the conclusion.

*Electronic address: inchiosa@nosc.mil. Web site: http://hpcweb.nosc.mil/hpc/sr/
†Electronic address: bulsara@nosc.mil. Web site: http://hpcweb.nosc.mil/hpc/sr/
‡Electronic address: gammaitoni@perugia.infn.it. Web site: http://www.pg.infn.it/sr/

II. PHENOMENOLOGICAL DESCRIPTION

We start with a simple phenomenological model of a purely deterministic situation. Consider a periodic signal $A\sin\omega t$ applied to a generic bistable potential $U(x)$. The signal is assumed to be of amplitude barely sufficient to achieve switching between the two stable states of the potential, which we assume to be asymmetric. We shall be concerned only with the dichotomous output $f(t)$ over a single period T of the signal, where we define

$$f(t)=f_0 \quad 0\leqslant t<\Theta$$
$$=0 \quad \Theta\leqslant t<T. \tag{1}$$

Clearly, the residence times Θ and $T-\Theta$ in the two stable states are functions of the asymmetry of the system: for a symmetric potential, $\Theta=T/2$. We now Fourier analyze $f(t)$

$$f(t)=\frac{a_0}{2}+\sum_{k=1}^{\infty}\{a_k\cos(k\omega t)+b_k\sin(k\omega t)\}, \tag{2}$$

where we readily compute,

$$a_0\equiv\frac{2}{T}\int_0^T f(t)dt=\frac{2f_0\Theta}{T}$$

$$a_k\equiv\frac{2}{T}\int_0^T f(t)\cos(k\omega t)dt=\frac{f_0}{\pi k}\sin(k\omega\Theta)$$

$$b_k\equiv\frac{2}{T}\int_0^T f(t)\sin(k\omega t)dt=\frac{f_0}{\pi k}[1-\cos(k\omega\Theta)].$$

Clearly, for a symmetric potential ($\Theta=T/2$), only the odd multiples of ω will be present. From the above expressions, the spectral amplitude at $k\omega$ is given by the absolute value of

$$M_k=\frac{f_0}{\pi k}\{\sin^2(k\omega\Theta)+[1-\cos(k\omega\Theta)]^2\}^{1/2}=\frac{2f_0}{\pi k}\sin\frac{k\omega\Theta}{2}, \tag{3}$$

where we will be interested in the absolute value only. A plot (Fig. 1) of $|M_k|$ over the interval $T/2\leqslant\Theta\leqslant T$ reveals multiple maxima with the number of maxima being $k/2$ and $(k+1)/2$ for even and odd k, respectively. The locations of these maxima are readily found from the condition $k\omega\Theta=n\pi$ (n odd). We observe that the fundamental ($k=1$) has a single maximum for $\Theta=\Theta_1=T/2$ corresponding to the symmetric case, the first harmonic ($k=2$) has a single maximum for $\Theta=\Theta_2=3T/4$, the $k=3$ harmonic has maxima at $\Theta=\Theta_3=5T/6,T/2$, the $k=4$ harmonic at $\Theta=\Theta_4=7T/8,5T/8$, and so on. Note (see Fig. 1) that the spectral amplitudes with odd k have a maximum at $\Theta=T/2$ (corresponding to the symmetric potential case), while ones with even k vanish in this case.

The extension to the noisy case is achieved by introducing the mean residence times $\langle t_l\rangle$ and $\langle t_r\rangle$ in the left and right states of the potential (the left well has the shallower minimum). For convenience, these may be computed in the absence of the periodic signal; the presence of the signal affects these mean times only slightly [6] for weak signal amplitudes. We then postulate that to achieve a maximum in a given spectral amplitude $|M_k|$ (assuming the output to be approximately periodic), we must achieve $\langle t_r\rangle=\Theta_k$ and $\langle t_l\rangle=T-\langle t_r\rangle$. For the first few harmonics this yields immediately $\langle t_l\rangle=T/2=\langle t_r\rangle$ for $k=1$ (this is the classical frequency-matching condition for stochastic resonance), $\langle t_l\rangle=T/4$ and $\langle t_r\rangle=3T/4$ for $k=2$, etc. In fact, we find a precise matching of stochastic and deterministic time scales for *every* frequency $k\omega$ whenever the spectral amplitude $|M_k|$ possesses a maximum. At frequency $k\omega$ we may write the general conditions for these ''resonances'' as

$$\langle t_l\rangle=\frac{n}{k}\frac{T}{2},\quad \langle t_r\rangle=T-\langle t_l\rangle,\quad \frac{\langle t_l\rangle}{\langle t_r\rangle}=\frac{n/2k}{1-n/2k}, \tag{4}$$

where n is odd and $1\leqslant n\leqslant k$. This leads to an elegant pattern of numbers (shown in Table I for $k=1,2,\ldots,9$) which exposes a precise matching of stochastic (the mean residence times) and deterministic (the signal period) time scales that must exist to obtain the (multiple) resonances (as a function

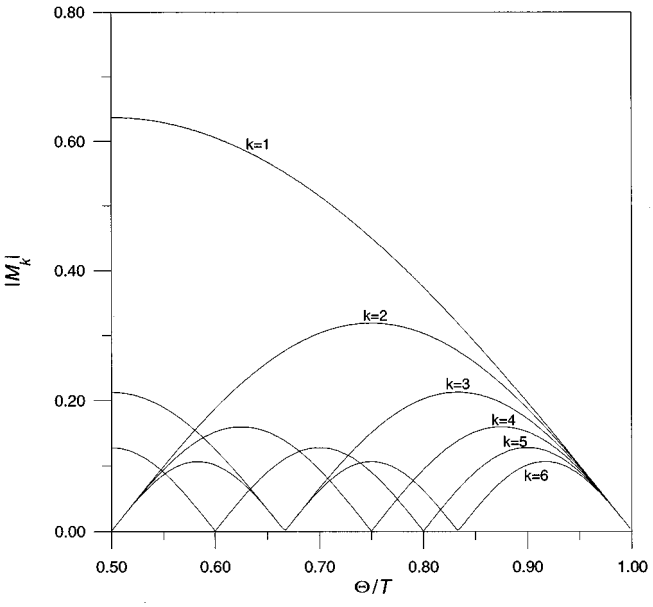

FIG. 1. Spectral amplitudes at frequency $k\omega$, $k=1,2,\ldots,6$ in the output PSD for the purely deterministic case, as computed from the phenomenological theory [Eq. (3)] with $f_0=1$. The horizontal scale represents the degree of asymmetry as quantified by the ratio Θ/T.

TABLE I. Mean residence time ratios which maximize the spectral amplitude at frequency $k\omega$.

k	$\langle t_l\rangle/\langle t_r\rangle$								
1	$\frac{1}{1}$								
2		$\frac{1}{3}$							
3	$\frac{3}{3}$		$\frac{1}{5}$						
4		$\frac{3}{5}$		$\frac{1}{7}$					
5	$\frac{5}{5}$		$\frac{3}{7}$		$\frac{1}{9}$				
6		$\frac{5}{7}$		$\frac{3}{9}$		$\frac{1}{11}$			
7	$\frac{7}{7}$		$\frac{5}{9}$		$\frac{3}{11}$		$\frac{1}{13}$		
8		$\frac{7}{9}$		$\frac{5}{11}$		$\frac{3}{13}$		$\frac{1}{15}$	
9	$\frac{9}{9}$		$\frac{7}{11}$		$\frac{5}{13}$		$\frac{3}{15}$		$\frac{1}{17}$

of asymmetry) at the frequencies $k\omega$ when the system is noisy. We now explore the resonance behavior in a specific system, the rf SQUID loop.

III. THE RF SQUID LOOP

The standard rf SQUID loop is a superconducting loop into which a single Josephson junction has been inserted [7]. The dynamics are multistable with the magnetic flux through the superconducting loop being quantized in units of the flux quantum $\Phi_0 \equiv h/2e$. In the presence of the junction, the magnetic flux Φ through the loop, in response to an applied time-dependent magnetic flux Φ_e, evolves according to the dynamics [7],

$$\left(LC\frac{d^2}{dt^2} + \tau_L \frac{d}{dt} + 1 \right) \frac{\Phi(t)}{\Phi_0} + \frac{\beta_s}{2\pi} \sin \frac{2\pi\Phi(t)}{\Phi_0} = \frac{\Phi_e(t)}{\Phi_0}, \quad (5)$$

where L and C are the loop inductance and capacitance, $\tau_L \equiv L/R_J$ (R_J being the normal state resistance of the junction), and the parameter $\beta_s \equiv 2\pi L i_c/\Phi_0$ (i_c is the junction critical current) controls the hysteretic behavior of the device: the SQUID output is hysteretic for $\beta_s > 1$, i.e., the steady state Φ vs Φ_e curves are multivalued. In most practical applications, the SQUID loop is shunted by a low resistance in order to remove hysteresis in the voltage-current characteristic of the junction [7]; this process effectively renders the link capacitance C extremely small so that the inertial term in Eq. (5) may be neglected. Transforming to the normalized state variable $x(t) \equiv \Phi(t)/\Phi_0$, we may write the dynamics (5) in the ''particle-in-a-potential'' form,

$$\tau_L \dot{x} = -\frac{\partial U(x)}{\partial x} + \eta(t) + y(t), \quad (6)$$

where the dot denotes time differentiation, and the potential function

$$U(x) = \frac{1}{2}(x - x_0)^2 - \frac{\beta_s}{4\pi^2} \cos(2\pi x), \quad (7)$$

is multistable when $\beta_s > \beta_{sc}$, where $\beta_{sc} = 1$ for $x_0 = 0$. We have expressed the (normalized) external flux Φ_e/Φ_0 as the sum of three terms: a symmetry-breaking dc term x_0 [which we incorporate into $U(x)$], an ac term $\eta(t) = A\sin(\omega t + \theta)$ with θ being a (often assumed random) phase factor, and a noise term $y(t)$. Typically the time constant $\tau_L \approx 10^{-12}$ sec, so that with the exception of the (internal) thermal noise, which is assumed negligible for the purposes of this paper, any externally applied noise will usually have a bandwidth far smaller than the SQUID bandwidth τ_L^{-1}. This is even more the case in experimental setups wherein a resistive shunt must often be placed across the SQUID to filter out high-frequency noise. The LR circuit formed by the shunt resistance and the loop inductance results in a low-pass filter which decreases the input noise bandwidth even further [8]. Hence, we must take $y(t)$ to be zero-mean Gaussian *exponentially correlated* noise; it may be modeled via a white-noise-driven Ornstein-Uhlenbeck (OU) process [9]

$$\dot{y} = -\tau^{-1} y + \sigma F(t), \quad (8)$$

where $F(t)$ is zero-mean ''white'' noise with autocorrelation $\langle F(t)F(t+s)\rangle_t = \delta(s)$ and τ is the correlation time of the ''colored'' noise $y(t)$. Then, one easily verifies [9] that $y(t)$ has zero mean and autocorrelation function $\langle y(t)y(t+s)\rangle_t = \langle y^2\rangle e^{-|s|/\tau}$, whence the ''white'' limit, corresponding to delta-correlated noise, is realized when $\tau \to 0$. The colored noise has variance $\langle y^2\rangle = \sigma^2\tau/2$ [we reiterate that $y(t)$ has units of normalized magnetic flux].

It is convenient to prebias the SQUID loop so that the potential (7), for $\beta_s > 1$, is centrally bistable with possible outlying metastable states. This is accomplished [8] by incorporating a dc bias $m/2$ (m odd) in the potential: we replace x_0 by $x_0 + m/2$. Assuming the signal and noise to be very slow compared to the well-relaxation time (the standard adiabatic assumption), we may incorporate the signal $\eta(t)$ and the noise $y(t)$ into the potential function $U(x)$ as well, writing Eq. (6) in the form $\tau_L \dot{x} = -\partial U_e(x)/\partial x$ where the potential function U_e is now given by

$$U_e(x(t)) = \frac{1}{2}\left(x - x_0 - \frac{m}{2} - y(t) - \eta(t) \right)^2 - \frac{\beta_s}{4\pi^2} \cos(2\pi x). \quad (9)$$

It is worthwhile to note that for the very small time constants τ_L that characterize real SQUIDs, the adiabatic assumption is expected to be a very good one, breaking down for input signals or input noise with power at very high frequencies (approaching τ_L^{-1}). The thermal background noise in the sensor is indeed broadband [7] but far smaller in magnitude than ambient environmental noise that limits practical SQUIDs. The environmental noise usually has a bandwidth less than τ_L^{-1}. As already stated, we neglect the thermal background noise throughout this work. Finally, we assume that the signal amplitude A is too weak to allow switching between the stable states of the potential to occur in the absence of the noise.

The fixed points of the effective potential may be computed in the absence of the noise [i.e., $y(t) = 0$] by setting $\partial U_e/\partial x = 0$ and solving the resulting transcendental equation via a perturbation expansion to leading order in x_0 and $\eta(t)$. We then obtain

$$x_u = \frac{m}{2} + \frac{x_0 + \eta(t)}{1 - \beta_s} \quad (10)$$

for the central (unstable) fixed point, and

$$x_1 = \frac{m-1}{2} + \frac{x_0 + \eta(t) + 1/2}{1 + \beta_s},$$

$$x_2 = \frac{m+1}{2} + \frac{x_0 + \eta(t) - 1/2}{1 + \beta_s} \quad (11)$$

for the stable fixed points to the left (x_1) and right (x_2) of x_u. We note that the above expressions are not valid in the $x_0 \to 1/2$ limit in which the central bistable structure of the potential $U(x)$ disappears (in fact, the theoretical computations of the power in various harmonics also break down in this limit). The theoretical and simulation results are identical for any odd m, and are reflected about the vertical axis

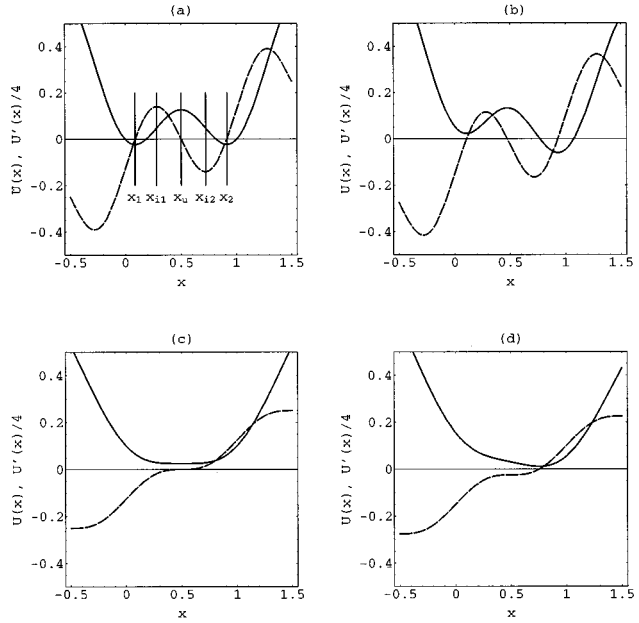

FIG. 2. Potential $U(x)$ (solid curve) and its derivative $U'(x)$ (dashed curve, scaled by 1/4 for plotting convenience) for (a) $\beta=5$, $x_0=0$, (b) $\beta=5$, $x_0=0.1$, (c) $\beta=1$, $x_0=0$, (d) $\beta=1$, $x_0=0.1$.

for $-1/2\leqslant x_0\leqslant 0$. Any other x_0 may be mapped into the range $-1/2\leqslant x_0\leqslant 1/2$ by modifying m.

In Fig. 2 we plot the potential $U(x)$ and its gradient $\frac{1}{4}\partial U/\partial x$ (the factor $\frac{1}{4}$ is introduced for scaling convenience in the figure) for different values of the nonlinearity parameter β_s and the dc asymmetry x_0. Clearly, the (generalized) inverse gradient function also represents the input-output characteristic of the device. The central bistable structure of the potential (for $\beta_s>1$, $x_0=0$) is readily apparent. The intersection(s) of the gradient term with the horizontal axis yield the extrema of the potential and the multivalued, hysteretic character of the input-output characteristic (picture the gradient function rotated 90° and flipped) corresponds to the bistable structure of the potential. The extrema of the gradient correspond to the points of inflexion [see Eq. (12) below] of the potential. For the asymmetric case (corresponding to nonzero x_0), we observe a skewing of the potential, accompanied by unequal areas enclosed between the gradient term and the horizontal axis. Although we have shown only the central well(s) of the potential for a given β_s it is clear that (depending on the magnitude of β_s) we would, in general, obtain multiple zeros of the gradient function, corresponding to a multistable potential.

SR, defined in the conventional way via the maximum—as a function of input noise power—in the output power signal-to-noise ratio (SNR) at the fundamental frequency ω, has been observed in an experiment performed in 1992 [8]. Two separate experiments carried out in 1994 [10,11] have observed such resonance behavior in the spectral amplitudes of higher harmonics (including the even ones) when the symmetry-breaking dc signal x_0 is present. Numerical simulations that determined the output power in the $k=1-4$ harmonics of the SQUID model (6) were recently presented, along with an approximate theoretical computation of this output power for the $k=1,2$ harmonics [6]. Very good agreement was found between theory and numerical simulations. In what follows, we present a much fuller account of the theoretical calculation of the output power as well as new results which provide a guide for using the resonance behavior depicted in Fig. 1 in practical nonlinear dynamic devices.

IV. THE SQUID LOOP AS A TWO-STATE SYSTEM WITH ASYMMETRY

We now present an approximate theoretical calculation of the first two spectral amplitudes in the output PSD. Since $\tau_L\ll\tau$, the SQUID may be assumed to remain in its (nonequilibrium) steady state, making transitions (accompanied by the emission of a single flux quantum) only when the noise causes the currently occupied minimum to coincide with a point of inflexion that can be calculated via $(\partial^2 U_e/\partial x^2)=0$. A straightforward calculation yields the locations of the points of inflexion generated in place of the left and right minima when a transition between states occurs

$$x_{i1}=\frac{m-1}{2}+\frac{1}{2\pi}\cos^{-1}(-\beta_s^{-1}),$$

$$x_{i2}=\frac{m+1}{2}-\frac{1}{2\pi}\cos^{-1}(-\beta_s^{-1}). \tag{12}$$

Thus the noise must achieve the values

$$y_{c1,2}=x_{i1,2}-x_0-\frac{m}{2}-\eta(t)+\frac{\beta_s}{2\pi}\sin(2\pi x_{i1,2}) \tag{13}$$

to accomplish switching. Therefore, we model the SQUID as a two-state system with a hysteretic input-output characteristic having state probabilities $p_{1,2}(t)$ and master equations

$$\dot{p}_1=W_{21}p_2-W_{12}p_1,$$

$$\dot{p}_2=W_{12}p_1-W_{21}p_2, \tag{14}$$

where $p_1+p_2=1$ and W_{ik} denotes the transition rate from state i to state k. These rates are the approximate inverses of the mean passage times $\langle t_l\rangle$ and $\langle t_r\rangle$ introduced earlier. The transition rates are computed by solving [9] the first passage problem for the OU process (underpinning the noise) between the values y_{c1} and y_{c2}. For W_{12} we assume the presence of an absorbing boundary at y_{c2}, with y_{c1} being the start point. Then we have,

$$W_{12}^{-1}\approx T_{12}=2\sigma^{-2}\int_{y_{c2}}^{y_{c1}}e^{z^2/\sigma^2\tau}dz\int_{-\infty}^{z}e^{-z'^2/\sigma^2\tau}dz'$$

$$=2\tau\sqrt{\pi}\int_{u_{c2}}^{u_{c1}}e^{u^2}\Psi(u)du. \tag{15}$$

A corresponding expression may be obtained for W_{21}

$$W_{21}^{-1}\approx T_{21}=2\tau\sqrt{\pi}\int_{u_{c2}}^{u_{c1}}e^{u^2}\Psi(-u)du. \tag{16}$$

We have defined $\Psi(u)\equiv\frac{1}{2}[1+\mathrm{erf}(u)]$ and $u_{c1,2}\equiv y_{c1,2}/\sigma\sqrt{\tau}$; further, we have, for later notational conve-

nience, set $T_{12}\equiv\langle t_l\rangle$ and $T_{21}\equiv\langle t_r\rangle$. As expected, for $x_0=0$, we find $y_{c2}=-y_{c1}$ and $T_{12}=T_{21}$. The integrals in Eqs. (15), (16) may be expressed in terms of the imaginary error function $\mathrm{erfi}(z)=\mathrm{erf}(iz)/i$ and the generalized hypergeometric function ${}_pF_q(a_1,\ldots,a_p;b_1,\ldots,b_q;z)$

$$\int_{u_{c2}}^{u_{c1}} e^{u^2}\Psi(\pm u)\,du = \left[\frac{1}{4}\sqrt{\pi}\,\mathrm{erfi}(u)\pm\frac{{}_2F_2(1,1;\tfrac{3}{2},2;u^2)u^2}{2\sqrt{\pi}}\right]_{u_{c2}}^{u_{c1}}.$$

To compute the PSD of the SQUID output, we must first solve the system (14) for the state probabilities $p_{1,2}(t)$. Then, the two-state dynamics that characterize the SQUID may be well approximated by the global probability density function

$$P(x,t)\approx p_1(t)\,\delta(x-x_{10})+p_2(t)\,\delta(x-x_{20}), \tag{17}$$

where $x_{1,20}\equiv x_{1,2}|_{A=0}$ are the locations of the minima of the *unperturbed* potential (7). The mean value $\langle x(t)\rangle$ is obtained from

$$\langle x(t)\rangle=\int xP(x,t)dx=x_{10}p_1(t)+x_{20}p_2(t). \tag{18}$$

A general solution of Eq. (14) is beyond the scope of this paper. However, we are interested in the spectral amplitudes of the first two peaks ($k=1,2$) in the output PSD. Accordingly, we are interested only in an expansion of $\langle x(t)\rangle$ to include terms up to second order (i.e., the $k=2$ harmonic)

$$\langle x(t)\rangle=M_0+M_1\cos(\omega t+\phi_1)+M_2\cos(2\omega t+\phi_2), \tag{19}$$

where $\phi_{1,2}$ are phases that may have random components, and the amplitudes M_i are as yet undetermined. The autocorrelation function of the output is

$$K(s)\equiv\langle\langle x(t)x(t+s)\rangle\rangle_t\rightarrow\frac{1}{T}\int_0^T\langle x(t)\rangle\langle x(t+s)\rangle dt \tag{20}$$

in the $s\rightarrow\infty$ limit, $T=2\pi/\omega$ being the signal period. Using Eq. (19) we readily find

$$K(s)=M_0{}^2+\frac{M_1{}^2}{2}\cos(\omega s)+\frac{M_2{}^2}{2}\cos(2\omega s), \tag{21}$$

so that the powers at the frequencies ω and 2ω in the output PSD are, respectively, $M_1{}^2/2$ and $M_2{}^2/2$.

We solve the system (14) after expanding the transition rates to $O(A^2)$. Specifically, we define $u_{c1,20}\equiv u_{c1,2}|_{\eta(t)=0}$ and set

$$u_{c1,2}=u_{c1,20}-\eta'(t),\quad \eta'(t)\equiv A'\sin(\omega t+\theta), \tag{22}$$

with $A'\equiv A/\sqrt{2\langle y^2\rangle}$ being a natural (and convenient) perturbation expansion parameter; we expect the theory to be valid for $A'\ll 1$ and within the realm of the adiabatic approximation (see above). We now expand the transition rates as

$$W_{12}\approx\alpha_0+\alpha_1\eta'(t)+\alpha_2\eta'^2(t),$$

$$W_{21}\approx\beta_0+\beta_1\eta'(t)+\beta_2\eta'^2(t), \tag{23}$$

the expansion coefficients being obtained through a straightforward expansion of the transition rates

$$\alpha_0\equiv T_{120}{}^{-1},\quad \alpha_1\equiv-\frac{T'_{120}}{T_{120}^2},\quad \alpha_2\equiv-\frac{1}{2}\left(\frac{T''_{120}}{T_{120}^2}-2\frac{T'^2_{120}}{T_{120}^3}\right)$$

$$\beta_0\equiv T_{210}{}^{-1},\quad \beta_1\equiv-\frac{T'_{210}}{T_{210}^2},\quad \beta_2\equiv-\frac{1}{2}\left(\frac{T''_{210}}{T_{210}^2}-2\frac{T'^2_{210}}{T_{210}^3}\right) \tag{24}$$

where,

$$T_{120}\equiv T_{12}|_{\eta'(t)=0}=2\tau\sqrt{\pi}\int_{u_{c20}}^{u_{c10}}e^{u^2}\Psi(u)\,du$$

$$T'_{120}\equiv\left.\frac{\partial T_{12}}{\partial\eta'}\right|_{\eta'(t)=0}=2\tau\sqrt{\pi}\{e^{u_{c20}^2}\Psi(u_{c20})-e^{u_{c10}^2}\Psi(u_{c10})\}$$

$$T''_{120}\equiv\left.\frac{\partial^2 T_{12}}{\partial\eta'^2}\right|_{\eta'(t)=0}=4\tau\sqrt{\pi}\{u_{c10}e^{u_{c10}^2}\Psi(u_{c10})-u_{c20}e^{u_{c20}^2}\Psi(u_{c20})\}$$

$$T_{210}\equiv T_{21}|_{\eta'(t)=0}=2\tau\sqrt{\pi}\int_{u_{c20}}^{u_{c10}}e^{u^2}\Psi(-u)\,du$$

$$T'_{210}\equiv\left.\frac{\partial T_{21}}{\partial\eta'}\right|_{\eta'(t)=0}=2\tau\sqrt{\pi}\{e^{u_{c20}^2}\Psi(-u_{c20})-e^{u_{c10}^2}\Psi(-u_{c10})\}$$

$$T''_{210}\equiv\left.\frac{\partial^2 T_{21}}{\partial\eta'^2}\right|_{\eta'(t)=0}=4\tau\sqrt{\pi}\{u_{c10}e^{u_{c10}^2}\Psi(-u_{c10})-u_{c20}e^{u_{c20}^2}\Psi(-u_{c20})\}. \tag{25}$$

We now formally integrate the first equation in Eq. (14), ignoring the initial condition term which vanishes in the $t\rightarrow\infty$ limit

$$p_1(t)=g^{-1}(t)\int_{t_0}^{t}W_{21}(t')g(t')dt', \tag{26}$$

where

$$g(t)\equiv\exp\left\{\int^t[\alpha+\beta\eta'(t')+\gamma\eta'^2(t')]dt'\right\}, \tag{27}$$

with $\alpha\equiv\alpha_0+\beta_0$, $\beta\equiv\alpha_1+\beta_1$, $\gamma\equiv\alpha_2+\beta_2$. Performing the integration in Eq. (27) and expanding the result to $O(A'^2)$ we find,

$$g(t)\approx e^{\zeta t}\left\{1-\frac{\beta A'}{\omega}\cos(\omega t+\theta)-\frac{\gamma A'^2}{4\omega}\sin(2\omega t+\theta)+\frac{\beta^2 A'^2}{2\omega^2}\cos^2(\omega t+\theta)\right\}$$

$$g^{-1}(t)\approx e^{-\zeta t}\left\{1+\frac{\beta A'}{\omega}\cos(\omega t+\theta)+\frac{\gamma A'^2}{4\omega}\sin(2\omega t+\theta)+\frac{\beta^2 A'^2}{2\omega^2}\cos^2(\omega t+\theta)\right\}, \tag{28}$$

where $\zeta\equiv\alpha+\gamma A'^2/2$. Substituting these expressions into Eq. (26), we may carry out the integration, with $t_0\to-\infty$. After considerable simplification we finally arrive at

$$p_1(t)=\frac{\beta_0}{\zeta}+A'\frac{\beta_0\beta-\beta_1\alpha}{\alpha(\alpha^2+\omega^2)^{1/2}}\cos(\omega t+\phi_1+\theta)+\frac{A'^2}{4\omega^2}(P_c^2+P_s^2)^{1/2}\cos(2\omega t+\phi_2+\theta)+\frac{A'^2}{4\omega^2}P_0, \tag{29}$$

where θ is the (in general, random) initial phase and,

$$\phi_1\equiv\tan^{-1}(\alpha/\omega),\quad \phi_2\equiv\tan^{-1}(P_s/P_c),$$

$$P_c\equiv(\alpha^2+4\omega^2)^{-1}\{\alpha(\beta_0\beta^2-2\omega^2\beta_2)+2\omega^2(\beta_0\gamma+2\beta_1\beta)\}+\beta(\alpha^2+\omega^2)^{-1}\left\{\frac{\beta_0\beta\omega^2}{\alpha}-2\omega^2\beta_1-\beta_0\beta\alpha\right\}$$

$$P_s\equiv(\alpha^2+4\omega^2)^{-1}\{2\omega(\beta_0\beta^2-2\omega^2\beta_2)-\alpha\omega(\beta_0\gamma+2\beta_1\beta)\}+\omega(\alpha^2+\omega^2)^{-1}\times\left\{2\alpha\beta\beta_1-2\beta_0\beta^2+\frac{\beta_0\gamma}{\alpha}(\alpha^2+\omega^2)\right\}$$

$$P_0\equiv\frac{\beta_0\beta^2+2\omega^2\beta_2}{\alpha}-\frac{2\beta}{\alpha^2+\omega^2}(\beta_1\omega^2+\alpha\beta\beta_0).$$

Then, using Eqs. (17) and (19), we arrive at the expressions

$$M_1=A'(x_{10}-x_{20})\frac{\beta_0\beta-\beta_1\alpha}{\alpha(\alpha^2+\omega^2)^{1/2}},$$

$$M_2=\frac{A'^2}{4\omega^2}(x_{10}-x_{20})(P_c^2+P_s^2)^{1/2}. \tag{30}$$

We have already shown [6] that the expressions (30) agree very well with direct numerical simulations of the system (5) and (8), as well as the two-state system (23). In particular, we have seen that the two-state approximation that is widely used in adiabatic treatments of SR [1,12] is a very good approximation to the SQUID dynamics because of the essentially steady-state nature of Eq. (5) predicated by the small time constant τ_L. Hence, we have been able to treat the problem as a first passage problem of the *noise* rather than the full dynamics (5) (the latter problem would be analytically intractable). We now analyze the expressions (30) under different circumstances.

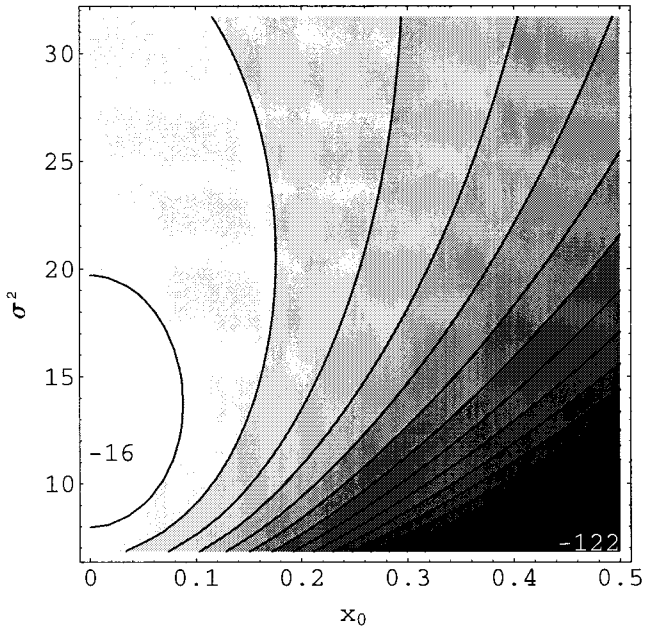

FIG. 3. Contour plot of SQUID output power $M_1^2/2$ (in dB) at the driving frequency ω vs asymmetrizing dc signal x_0 and noise parameter (in units of $\sec^{-1}$) σ^2. Other parameters: $\beta_s=5$, $A=0.1$, $\omega=10$, $\tau=0.01$, $m=1$. Numbers within contour plot mark the maximum and minimum power points (in dB).

In Figs. 3 and 4 we show the powers [computed via the theoretical expressions (30)] $M_1^2/2$ and $M_2^2/2$ in the first two peaks ($k=1,2$) in the output PSD as functions of the dc offset x_0 and the input noise parameter σ^2. The known signal amplitude is held constant, as is the SQUID nonlinearity parameter β_s; this results in a constant ratio $A/\Delta U_0$, where

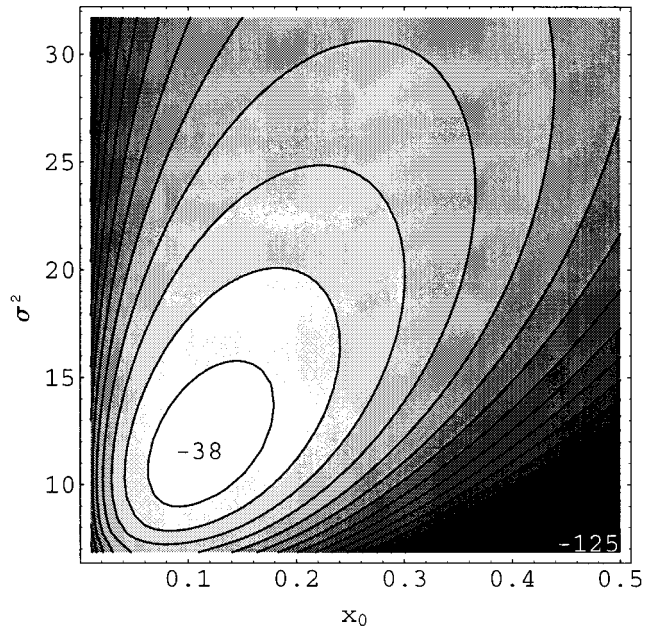

FIG. 4. Contour plot of SQUID output power $M_2^2/2$ (in dB) at frequency 2ω vs asymmetrizing dc signal x_0 and noise parameter (in units of $\sec^{-1}$) σ^2. Other parameters as in Fig. 3. Numbers within contour plot mark the maximum and minimum power points (in dB).

ΔU_0 is the height of the potential barrier of the central bistability of our problem, in the absence of any skewing (i.e., for $x_0=0$). In $M_1^2/2$ (the SQUID output power at frequency ω) the basic SR effect is readily visible: for $x_0=0$, the power displays a clear maximum as a function of the input noise power. The power in the first harmonic, $M_2^2/2$, vanishes as $x_0\to 0$ as expected. However, for $x_0\neq 0$ this power, like the power at the fundamental, displays a maximum as a function of the input noise power; also, a maximum is seen as a function of x_0, and the location of this maximum depends on the noise power. These results have also been demonstrated in bistable systems driven by white noise [2]. The powers do not display a strong dependence on ω; however, the adiabatic approach does require that $f\equiv(\omega/2\pi)\ll\tau^{-1},\tau_L^{-1}$.

It is important to note that the central bistable structure of the potential disappears for $x_0=1/2$; therefore, close to this point the bistable model upon which our theoretical calculation is based begins to break down. In [6] we performed numerical computations of the powers $M_k^2/2$ up to $k=4$. We found that the bistable theory agreed well with numerical simulations of a SQUID with a two-state-filtered output, even for x_0 close to 1/2. The bistable theory also agrees well with numerical simulations of a SQUID loop with an unfiltered, analog output, except for $k=1$ with x_0 approaching 1/2. For this case the bistable theory, by ignoring the motion *within* the deepest (and approximately parabolic) potential well, underestimates the output power at frequency ω, although it does accurately estimate the power at 2ω, which arises primarily from interwell motion.

V. DISCUSSION

It is worth starting this section by reiterating that the theory of this paper has been shown [6] to be in excellent agreement with numerical simulations on the SQUID equations (6) and (8). In fact, the matchings (4) of deterministic and stochastic time scales that characterize this higher-order resonant behavior have been shown to hold true (qualitatively) for the particular example system (the SQUID loop) considered here.

What are the limits of validity of the theoretical calculations presented here? In classical SR treatments [1,3,12] the noise $y(t)$ is taken to be white and a perturbation modification of the Kramers rate used to compute the transition rate. Note that the Kramers rate in its ''Arrhenius'' form [9] is, itself, an approximation strictly valid for low-noise intensity and large potential barrier heights; similar restrictions still apply to the system at hand, if one wishes to describe the dynamics via a Markov process (see below). The remaining approximations that we have employed are the perturbation expansion (23) in powers of A' and the adiabatic approximation which assumes the ac bias signal frequency to be the slowest rate in the dynamics. Both these approximations are well satisfied in the theory and simulations presented here. In fact, we would expect the theory to yield acceptable results even when the periodic signal is slightly suprathreshold, i.e., when deterministic switching is possible, as long as the noise has values such that $A'\ll 1$, in this case the system is apt to follow the behavior of the phenomenological two-state system discussed in Sec. II. However, when the input signal and/or noise terms become too large, the SQUID is able to make excursions to outlying minima of the potential (9) and the system can no longer be approximated by centrally bistable dynamics; in this case the theory breaks down. For the adiabatic criterion to be satisfied we should have $f\ll\tau_L^{-1},\tau^{-1}$. Simultaneously, the system and signal parameters should be chosen so that $f\ll W_{12},W_{21}$, else our approach of assuming the SQUID to be in its steady state and essentially tracking the noise dynamics [via the computation of the transition rates in Eq. (14)] breaks down. Certainly, the first of these conditions holds true for the frequencies considered in this work, and for those that are likely to be encountered in many practical applications. When the signal frequency exceeds the noise bandwidth, the adiabatic approximation begins to unravel; however, for signal frequencies not too far removed from the noise bandwidth, the theory can be shown to yield the correct qualitative behavior, although agreement such as that reported in [6] will not be achieved in this case.

The above comments are directly connected to the validity of the representation of the SQUID dynamics via a dichotomous Markov process. Typically, the residence times distribution for the process may be computed directly (see, e.g., [4]) from the probability density function (17). For a Markov process, the residence times distribution is expected to be a decaying exponential at long times, at least. In general, one would realize such dynamics if the transition rates W_{ik} were constant. The adiabatic assumptions are, therefore, critical to the success of the Markov approximation; by assuming the signal frequency to be much smaller than other characteristic system frequencies, we are assuming the transition rates to be quasistationary. At the same time, successive transitions or ''spikes'' should not be correlated; assuming very weak [as quantified in Eq. (22)] signal amplitudes and weak (compared to the barrier height) noise intensities assures this to be the case, even though the noise correlation time is typically greater than the SQUID constant τ_L (the exception being thermal noise). When the aforementioned conditions are met, the dynamics are approximately Markovian; we have already seen [6] that the approximations provide highly accurate representations of the actual dynamics.

The results of this paper (which explain very well the experimental observations of [10] and [11]) should be applicable to generic bistable and (in special situations such as described here in connection with the SQUID) multistable systems with broken symmetry. Many nonlinear detectors suffer from significant low-frequency noise limitations (the noise may be internal, e.g., $1/f$, or external). By carefully selecting the frequency ω of the *known* bias signal, the detection may be shifted to a more acceptable part of the frequency spectrum. Then, in a detector that has an *a priori* symmetric potential, the appearance of the even multiples of ω in the output PSD, together with the change in the spectral amplitudes $|M_k|$ in the presence of the symmetry-breaking signal (which may be dc, or have a single frequency in which case one looks at the properties of combination tones in the output PSD), may be used to detect or estimate the weak target signal. This idea was, in fact, demonstrated in laboratory experiments carried out with a specially designed ''SR SQUID'' [10] assuming only internal white noise, as well as a conventional rf SQUID [11] using externally applied correlated noise. In actual remote sensing applications, one of-

ten knows *a priori* the spectral characteristics of the background noise. In this case, it is clearly of benefit to be able to adjust the potential barrier height ΔU_0 and/or the amplitude of the known bias signal so as to achieve the highest possible sensitivity. In fact, the peak powers in Figs. 3 and 4 increase as the ratio $A/\Delta U_0$ increases; hence, for optimum detection, it might be advisable to adjust the bias signal amplitude A such that it is almost at the threshold for deterministic switching, with the barrier height already selected to maximize the output SNR. The barrier height may be adjusted by either fabricating a SQUID with a certain nonlinearity parameter β_s (in turn, this parameter depends on the junction critical current I_c and the loop inductance L) or by introducing an asymmetrizing dc flux x_0, as discussed in this paper. It is important to note that theory predicts the best possible output SNR at the fundamental for zero barrier height, corresponding to the linear system case; however, other practical considerations may render this mode of detection impractical in real devices, e.g., the rf SQUID detector wherein background noise and a low slew rate make detection of very weak signals via conventional techniques difficult, in the presence of even moderate amounts of noise. For practical applications it would be desirable to be able to compute *a priori* the receiver operating characteristics of the sensor [13], which are plots of detection vs false alarm probabilities for different detection thresholds. This calculation is currently in progress. Note also that the frequency shifting idea that is the focus of this paper applies exclusively to nonlinear systems; a linear sensor, for example, could not exploit this phenomenon.

ACKNOWLEDGMENTS

A.R.B. acknowledges support from the Office of Naval Research through Grant No. N0001496AF00002, the Internal Research program at NCCOSC, and NATO-CRG 931464. M.E.I. was supported in part by a Grant of HPC time from the DoD Major Shared Resource Center at WPAFB on the Intel PARAGON. We acknowledge helpful discussions with F. Marchesoni.

[1] For a good overview, see P. Jung, Phys. Rep. **234**, 175 (1994).

[2] R. Bartussek, P. Jung, and P. Hanggi, Phys. Rev. E **49**, 3930 (1994); P. Jung, R. Bartussek, in *Fluctuations and Order: The New Synthesis*, edited by M. Millonas (Springer-Verlag, New York, 1996); K. Lorincz, Z. Gingl, L. Kiss, and A. Bulsara (unpublished).

[3] For good overviews, see K. Wiesenfeld and F. Moss, Nature **373**, 33 (1995); A. Bulsara and L. Gammaitoni, Phys. Today **49**(3), 39 (1996).

[4] A. Bulsara, S. Lowen, and D. Rees, Phys. Rev. E **49**, 4989 (1994); A. Bulsara, T. Elston, C. Doering, S. Lowen, and K. Lindenberg, Phys. Rev. E **53**, 3958 (1996).

[5] L. Gammaitoni, F. Marchesoni, and S. Santucci, Phys. Rev. Lett. **74**, 1052 (1995).

[6] A. Bulsara, M. Inchiosa, and L. Gammaitoni, Phys. Rev. Lett. **77**, 2162 (1996).

[7] A. Barone and G. Paterno, *Physics and Applications of the Josephson Effect* (Wiley, New York, 1982).

[8] A. Hibbs, A. Singsaas, E. Jacobs, A. Bulsara, J. Bekkedahl, and F. Moss, J. Appl. Phys. **77**, 2582 (1995).

[9] See, e.g., C. Gardiner, *Handbook of Stochastic Methods*, (Springer-Verlag, Berlin, 1983).

[10] R. Rouse, S. Han, and J. Lukens, Appl. Phys. Lett. **66**, 108 (1995).

[11] *New Type of Magnetic Flux Sensor based on Stochastic Resonance in a Flux Quantized Superconducting Loop* (Quantum Magnetics Inc., 7740 Kenamar Ct., San Diego, CA, 1995).

[12] L. Gammaitoni, F. Marchesoni, E. Menichaella-Saetta, and S. Santucci, Phys. Rev. Lett. **62**, 349 (1989); B. McNamara and K. Wiesenfeld, Phys. Rev. A **39**, 4854 (1989).

[13] M. E. Inchiosa and A. R. Bulsara, Phys. Rev. E **53**, 2021R (1996).